Observation of dark exciton luminescence from ZnO nanocrystals in the quantum confinement regime

Sekika Yamamoto and Tomobumi Mishina
Department of Physics, Graduate School of Science, Hokkaido University, N10W8, 060-0810 Sapporo, Japan
(Received 31 October 2010; revised manuscript received 25 January 2011; published 22 April 2011)

Time-resolved luminescence measurements are performed on high-quality ZnO nanocrystals in a quantum confinement regime prepared by fast cooling and succeeding surface passivation. A very long luminescence lifetime of ∼0.1 μs, which is indicative of the existence of a dark exciton state, is observed. The temperature dependence of the lifetime and the luminescence peak energy is successfully accounted for by a thermal equilibrium model of excitonic dark and bright states.

DOI: 10.1103/PhysRevB.83.165435 PACS number(s): 78.67.Bf, 73.22.−f

I. INTRODUCTION

Zinc-oxide-based nanostructures have recently attracted attention due to their potential applications in spintronic and ultraviolet to violet light-emitting and other optical devices.[1–5] They can be obtained easily by sol-gel synthesis, chemical precipitation, colloidal synthesis, and the electrophoretic dissolution of a sacrificial anode. The ease of production by these methods is favorable for large-scale fabrication in actual applications.

However, the understanding of the electronic state in a ZnO nanocrystal (NC) with its size in the quantum confinement regime is insufficient compared to other II-VI semiconductor NCs, such as CdSe and CdS. In particular, the electronic-state evaluations, including the exchange interaction between electron and hole, are scarce. In CdSe NCs, it is widely accepted that the ground state of the electron-hole pair is optically forbidden (dark excitons).[6–10] This picture successfully explains the particle-size dependence of Stokes shift and the temperature dependence of the luminescence lifetime, and so on. With dark exciton in its ground state, the luminescence lifetime at low temperatures becomes very long because efficient radiative recombination occurs only when the excitons are thermally excited into the bright state. In CdSe NCs, the lifetime of the exciton at low temperatures has been observed to be around 1 μs (Refs. 8 and 9), which is much longer than the bulk lifetime of ∼1 ns. It has also been shown that the ground state of small CdS NCs is the dark exciton, which exhibits a long-lifetime luminescence.[10]

However, as far as we know, such long-lifetime luminescence reflecting a dark ground state has never been observed in ZnO NCs of quantum confinement size (with diameter $D < 5$ nm). Recently the electronic state in spherical ZnO NCs has been calculated under pseudopotential formalism.[11] According to the result, the ground state is a spin-forbidden dark state for a wide range of crystal sizes. The discrepancy between the theoretical and experimental results may be partly due to the crystal disorder existing in the real NCs that greatly modifies the excitonic state. The band-edge luminescence from ZnO NCs usually exhibits a large Stokes shift that is interpreted as a result of the localization of the electron to the surface or internal trap state.[12] Therefore, a higher-quality sample is needed to investigate the exact ground state of the electron-hole pair in ZnO NCs.

In this work, we apply an alternative method to prepare ZnO NCs of quantum confinement size and, as a result, we observe a band-edge luminescence with a very long lifetime at low temperatures that strongly implies that the ground state of the ZnO NCs is optically forbidden.

II. EXPERIMENTAL METHODS

Zinc oxide NCs are prepared as follows. First, 1.10 g of zinc acetate dehydrate ($ZnAc_2 \cdot 2H_2O$) is dissolved in 50 mL of absolute ethanol by boiling, and 0.29 g of lithium hydroxide monohydrate ($LiOH{\cdot}H_2O$) is dissolved in 50 mL of absolute ethanol ultrasonically. Typically, 10 mL of the Zn solution is heated to 70 °C before the same amount of LiOH solution, cooled at 0 °C, is poured under vigorous stirring. The solution is kept at room temperature for particle growth. After the desired particle size is attained, 200 mg of magnesium acetate tetrahydrate ($MgAc_2 \cdot 4H_2O$) is added into the solution and dissolved ultrasonically. The resulting solution is stored at room temperature for at least three days. After the addition of Mg salt, the particle growth is stopped and the suspension becomes very stable, even at room temperature. No turbidity is recognized after one year of storage at room temperature. We prepare four samples with variations of the average diameter from 3.2 to 3.5 nm. The average diameters of the samples are evaluated from the absorption-edge energies using Meulenkamp's empirical formula.[13] An x-ray-diffraction measurement for the dried sample shows clear evidence for the wurtzite structure of the crystal, and no other peaks such as zinc hydroxide[14,15] are recognized. The average diameters calculated from the diffraction linewidth using a modified Scherrer's formula[16] are consistent with those obtained from absorption measurements. The details of the sample preparation and the results of the x-ray diffraction are given in our previous paper.[17]

For time-resolved photoluminescence (PL) measurements, the third harmonics of a mode-locked Ti:sapphire laser, with a repetition rate of 80 MHz and a pulse duration of about 100 fs, is used for the excitation source. Typical time-averaged laser power density is 1 kW/cm^2. The detection of PL light is performed with a Hamamatsu C1587 streak camera system which has a time resolution of about 20 ps.

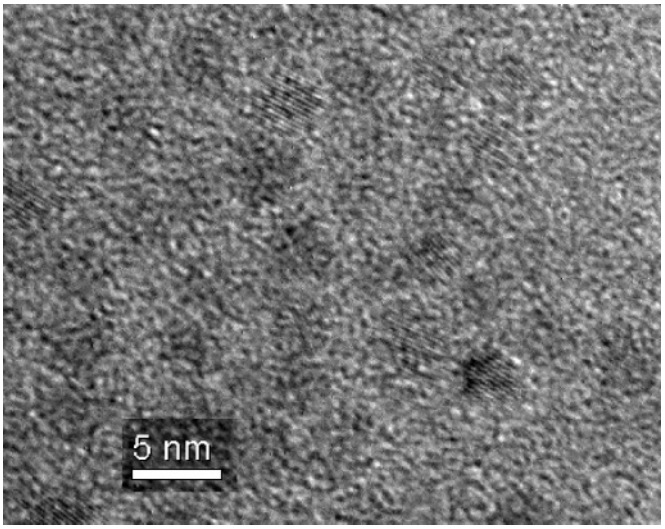

FIG. 1. TEM image of drop-cast ZnO nanocrystals. The crystal shape is recognized to be almost spherical, with average diameter ∼3 nm.

III. RESULTS AND DISCUSSION

Figure 1 shows a typical TEM image obtained for the drop-cast sample. The shapes of the NCs seen in the figure are nearly spherical, which is typical of the ZnO NCs of this size.[18,19] The average diameter evaluated from the TEM images is consistent with that obtained in x-ray diffraction.

Figure 2 shows typical absorption and PL spectra measured at room temperature. The absorption edge (which is energy that corresponds to the half height of the first peak) is observed at about 3.63 eV, which is 0.31 eV greater than the bulk value because of the quantum confinement effect.[20] The dependence of the absorption edge on the crystal size in ZnO NCs has been investigated by Meulenkamp and an empirical formula has been derived.[13] The NC size calculated using the formula is 3.2 nm for this sample, and it is in good agreement with that obtained by the x-ray diffraction and the TEM result. The band-edge PL shown by a solid line in the figure is slightly red-shifted from the absorption spectrum. The red shift of the PL from the absorption is generally called a Stokes shift. In this case, evaluating the precise Stokes shift from Fig. 2 is difficult because the absorption spectrum is much broader than the PL spectrum, and probably consists of several optical transitions with different energies. Therefore we evaluate the Stokes shift as the difference between the lower edges of the two spectra normalized at the peak intensities, as indicated by the arrow in the figure, and a value of 135 meV is obtained for this sample. In a general sense, such a large value of the Stokes shift should be at least partially attributed to a carrier trapping caused by some kind of disorder in the NC.

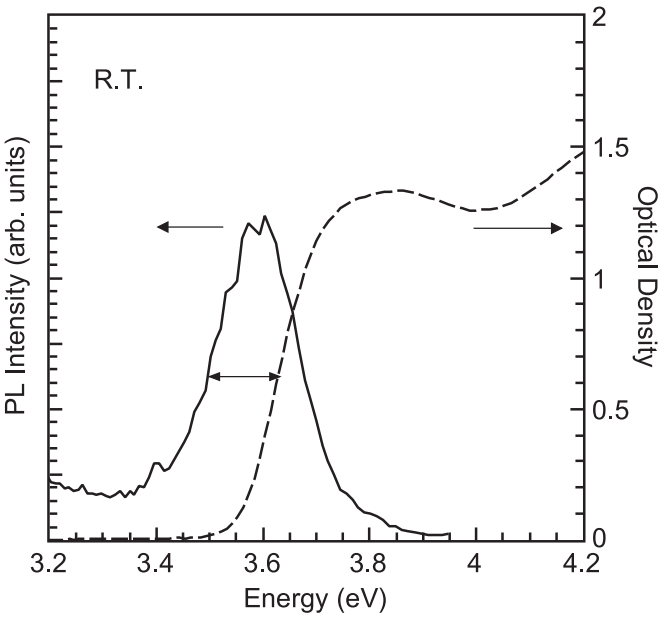

FIG. 2. Absorption (dashed line) and photoluminescence (solid line) spectra for the sample with average size of 3.2 nm measured at room temperature. The Stokes shift is estimated to be 135 meV as the difference between the lower edges of the two spectra.

Figure 3 shows a typical result of the time-resolved PL at 20 K detected by the streak camera. Two components with different peak energies and different lifetimes are recognized in the figure. One is at lower energy with a shorter lifetime and the other is at about 80-meV higher energy with a much longer lifetime. The component with a short lifetime has also been observed in other ZnO NCs and attributed to a near-band-edge PL in which one type of carrier is at a shallow trap.[21,22] The high-energy component has nonzero intensity at the negative time region because the lifetime of this component is longer than the repetition period of the laser system (12.5 ns in this case) and the long tails from the previous

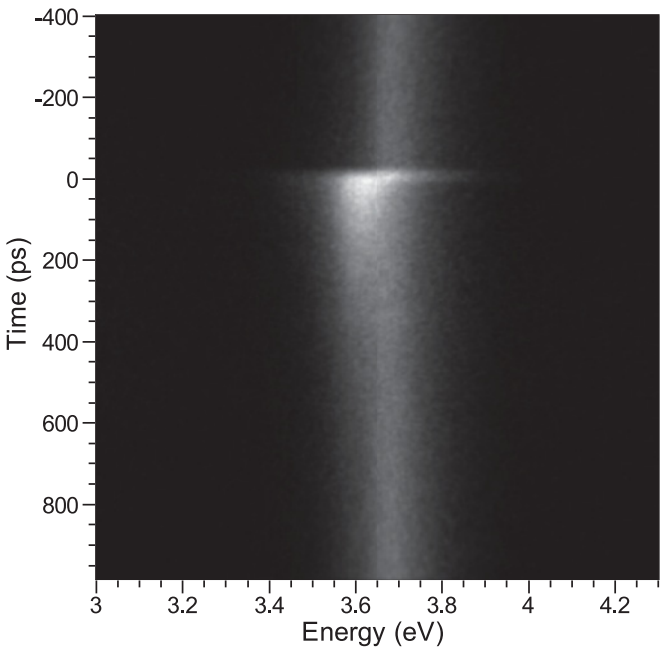

FIG. 3. Time-resolved luminescence at 20 K detected by the streak camera for the sample with average size of 3.2 nm. Two components with different peak energies and different lifetimes are recognized. The high-energy component with a very long lifetime has a signal intensity at the negative time region, which is a result of the superposition of the long tails from the previous pulse events onto the measurement time window.

pulse events are superposed in the measurement time window. We think that this component originates from the high-quality group of NCs in the specimen because higher luminescence energy (that is, smaller Stokes shift) and longer lifetime are generally considered as evidence of the higher quality of the semiconductor samples. For comparison, we also prepare a ZnO NC sample by the method introduced by Meulenkamp in which the precursor solutions are mixed dropwise at 0 °C. The result of the PL measurement shows no such long-lifetime luminescence. Therefore, we think that our sample preparation method, including fast cooling of the solution and succeeding passivation of the surface, increases the number of NCs with high optical quality.

The lifetime over 12 ns is much longer than the bulk free-exciton lifetime of 322 ps at 2 K.[23] The same kind of slow luminescence has been observed in CdSe and CdS NCs and they are attributed to dark excitons.[6,7,10] In the systems with dark exciton in the ground state, the radiative recombination occurs only when the excitons are thermally excited from the dark state to the bright state. This makes the luminescence lifetime at low temperatures much longer than that of bulk samples. As far as we know, the dark exciton state has never been observed in ZnO NCs. However, the smaller Stokes shift for the high-energy PL component suggests that the electronic state responsible for the luminescence is less affected by trapping potential and it should be much like the intrinsic state of the NC, and hence the very long lifetime observed here strongly implies that the intrinsic ground state of the exciton confined in the ZnO NC is optically forbidden.

To investigate the behavior of the high-energy component in detail, we decompose the luminescence spectrum into two components using a numerical fitting. We use the spectrum observed at the negative time region as the spectrum of the high-energy component. It is nearly a Gaussian shape with its tails slightly broadened at both sides, and we assume that it does not change significantly within its lifetime. For the low-energy component, a Gaussian spectral shape is assumed. The peak energy and the width of the Gaussian function are determined in a preliminary fitting procedure and assumed to be independent of time. The intensities of the two components are numerically adjusted to give the best fit at each time point. The results of the decomposition are shown in Fig. 4. At 20 K, two components have comparable intensities at $t = 0$ ps, while the spectrum at $t = 90$ ps shows a much decreased contribution from the high-energy component. This behavior is also recognizable in Fig. 3, where the intensity at the high-energy side shows a fast decrease within the time resolution of the measurement. The very fast decay just after the excitation has also been observed in the sample grown at 0 °C.[21] Therefore the fast decay can be attributed to the trapping of the excitons to a shallow trap that leads to the low-energy PL component, or the trapping to a nonradiative center in nonluminous particles. At 950 ps, the contribution of the low-energy component has almost vanished and the spectrum is dominated by

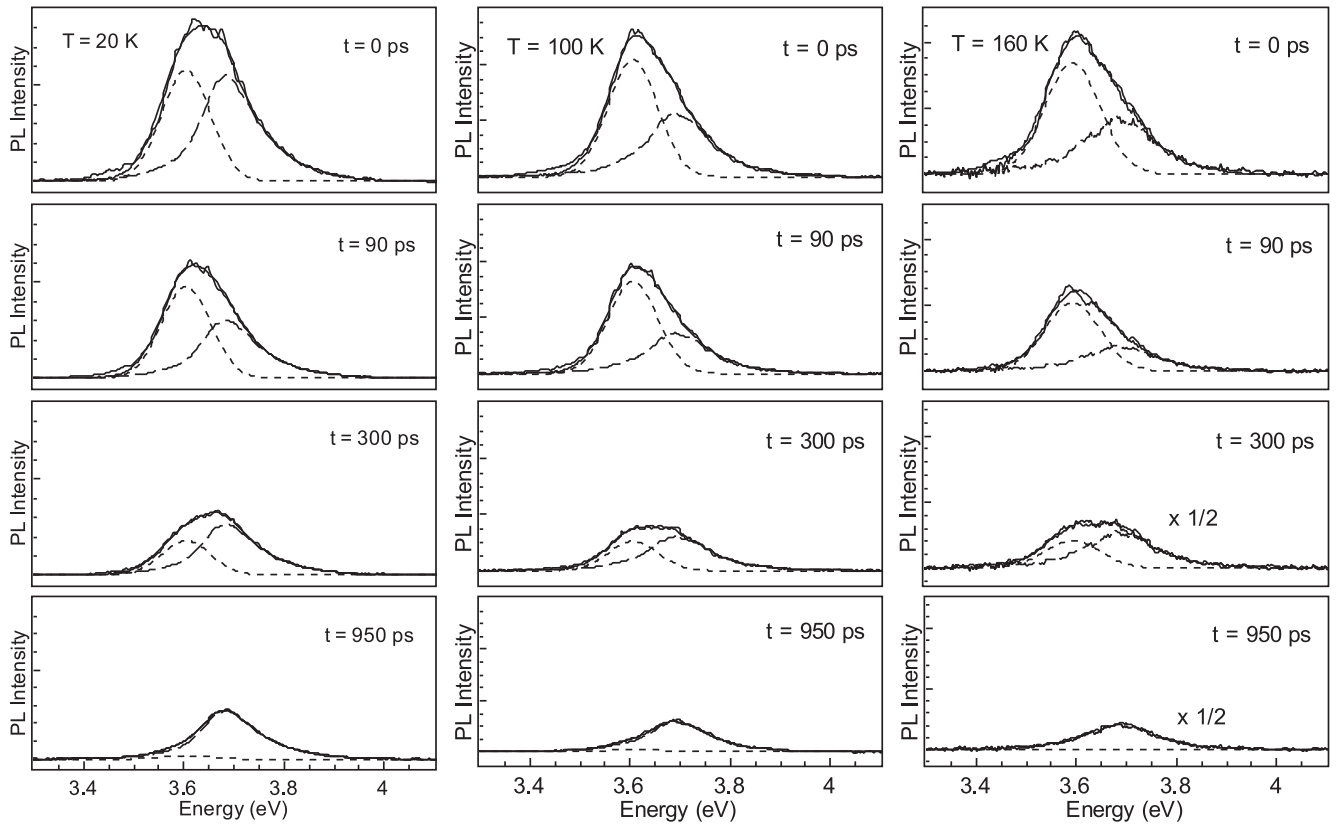

FIG. 4. The result of the spectrum decomposition at 20, 100, and 160 K. All spectra are successfully decomposed into two components. At all temperatures, the low-energy component fades away before 950 ps and the spectra become dominated by the high-energy component. Note that the spectrum at 950 ps is mostly composed of the superposed tail signals.

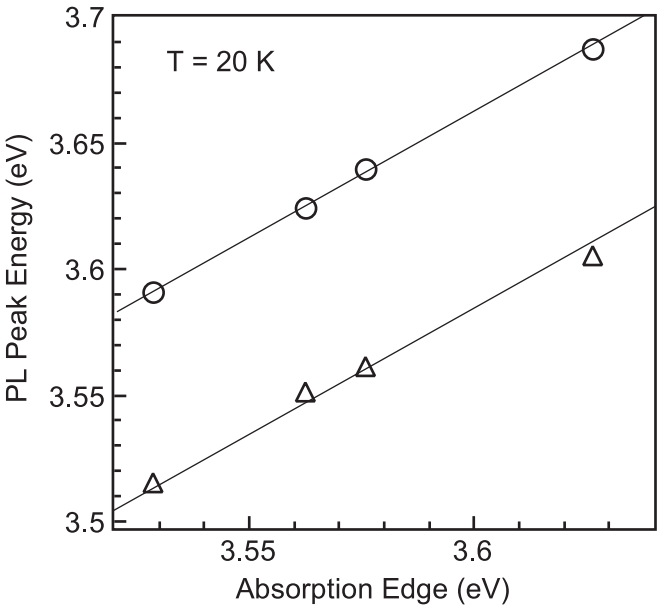

FIG. 5. The crystal size dependence of the peak energies of the two components. The horizontal axis shows absorption-edge energy at room temperature, which varies with the particle size as a reflection of the quantum confinement effect. Both of the peak energies are on the slope of unity, indicating that both components are related to the band-edge state of ZnO nanocrystals.

the high-energy component. At higher temperatures, the intensities of the high-energy component at $t = 0$ ps are decreased compared to the low-energy component. The reason for this is not clear, but we think that the origin for the fast decay just after the excitation should be related to a nonradiative recombination in optically poor particles, as discussed below, and the intensity reflects the thermal properties of their luminescence. One also sees in the figure that the intensity at 950 ps also depends on temperature. However, the intensity at this point in the time window mostly consists of the superposed tails of the previous pulse events, and the evaluation of the intensity is not straightforward.

Figure 5 shows the obtained peak energies of these two components for several samples with different average size. The energies are plotted against the absorption edge measured at room temperature, which varies with particle size as a reflection of the quantum confinement effect. It is observed that the peak energies are approximately on the lines with the slope of unity. This result unambiguously shows that both of these components originate from the band-edge-related states of the ZnO NCs.

Figure 6 shows the time profiles of the intensities obtained by the spectrum decomposition. The result for the low-energy component is shown in Fig. 6(a) and is approximated by a single exponential with a time constant of 220 ps. The slight deviation from the line after 500 ps depends on the fitting conditions and has less physical meaning. The temperature dependence of the decay time is shown in the inset and fitted by the usual thermal quenching model of $\tau \propto (A + B\exp[-E_{\rm nr}/k_B T])^{-1}$ with an activation energy $E_{\rm nr} = 34$ meV. The time profile of the intensity of the high-energy component is shown in Fig. 6(b). After the very fast

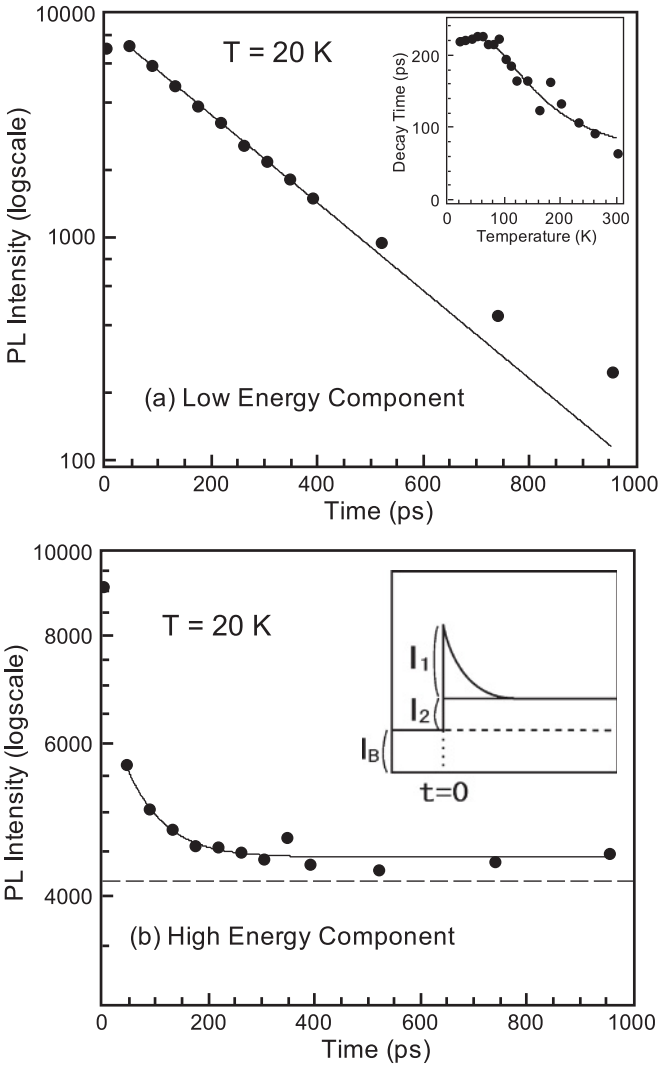

FIG. 6. The time profiles of the two components obtained from the spectrum decomposition at each time point. (a) The low-energy component decays almost exponentially. The temperature dependence of the lifetime is explained by the thermal quenching model as shown in the inset. (b) The high-energy component shows a steep decrease just after the excitation and then approaches the constant value above the background level (dashed line) composed of the superposed tail signals. The inset shows a schematic illustration of the model used to analyze the time profile including superposed signals.

decay at $t = 0$ mentioned in Fig. 4, a slower decay with a time constant of about 60 ps is observed, and after about 300 ps, the intensity becomes almost constant with the value just above the broken line. This line indicates the intensity at the negative time region, that is, the intensity of the superposed tail signals. As discussed above, we think that the slow decay after 300 ps is due to the luminescence associated with the dark exciton. Therefore, the intermediate decay with a 60-ps time constant should be attributed to the transition from the bright state to the dark state prior to the thermalization.

The time profile that contains the superposition of the tail signals is analyzed as follows. First, we assume that the decay

curve is approximated by a double exponential form of

$$I_0(t) = I_1 \exp[-\sigma_1 t] + I_2 \exp[-\sigma_2 t], \tag{1}$$

where the first term corresponds to the transition from the bright state to the dark state, and the second term corresponds to the radiative decay of the excitons. The values σ_1 and σ_2 are called decay rates and are inversely proportional to the lifetimes of the components. The second term is assumed to be very slow and to give the superposed intensity on the time profile. The contribution from the previous pulse events is then expressed as

$$\begin{aligned} I_s(t) &= \sum_{n=1}^{\infty} \left(I_2 \exp\left\{ -\sigma_2 \left[\left(n - \frac{1}{2} \right) T - t \right] \right\} \right. \\ &\quad \left. + I_2 \exp[-\sigma_2 (t + nT)] \right) \\ &= I_2 \frac{\exp\left[-\sigma_2 \left(\frac{1}{2} T - t \right) \right] + \exp[-\sigma_2 (t + T)]}{1 - \exp[-\sigma_2 T]}, \end{aligned} \tag{2}$$

where T is the repetition period of the laser system and the first term in the summation is a contribution from the return sweep of the streak camera, which must be taken into account in the systems without a synchronous blanking unit. If the decay rate σ_2 is small and the time window of the measurement is much shorter than T, the resulting curve $I_s(t)$ inside the window is almost time independent and σ_2 can be evaluated as $\sigma_2 \sim 2\ln(1 + I_2/I_B)/T$ where $I_B \equiv I_s(0)$ is measured as the signal intensity at the negative time region. The fitting function actually used to fit the decay profile after the initial fastest decay is

$$I(t) = I_1 \exp[-\sigma_1 t] + I_2 + I_B, \tag{3}$$

with I_B fixed to the measured value. We determined I_1, I_2, σ_1, and σ_2 at each temperature by fitting this function to the time profiles. The typical result of the fitting is shown by a solid line in the figure.

The temperature dependence of the parameters σ_2 and I_2 obtained by the fitting is shown in Fig. 7(a). The result clearly shows an increase of σ_2 with temperature, which is consistent with the thermal activation model from dark to bright state. The intensity I_2 is also observed to increase with temperature as shown in the inset. Therefore the increase of the decay rate reflects the enhancement of the oscillator strength, also consistent with the thermal excitation model. It is also observed in the figure that the decay rate σ_2 and the amplitude I_2 do not completely vanish at the low-temperature limit. This observation shows that the dark state is not truly dark but emits photons at a certain rate. If we assume a thermal equilibrium between the bright state and the slightly emitting dark state, the radiative decay rate is expressed as

$$\sigma = \frac{\sigma_d + \sigma_b \gamma e^{-\beta \Delta E}}{1 + \gamma e^{-\beta \Delta E}}, \tag{4}$$

and the center of the luminescence is

$$E = \frac{E_d \sigma_d + E_b \sigma_b \gamma e^{-\beta \Delta E}}{\sigma_d + \sigma_b \gamma e^{-\beta \Delta E}} \quad (\Delta E = E_b - E_d), \tag{5}$$

where σ_d and σ_b are the radiative decay rates for the dark and bright state, E_d and E_b are the energies of the luminescence

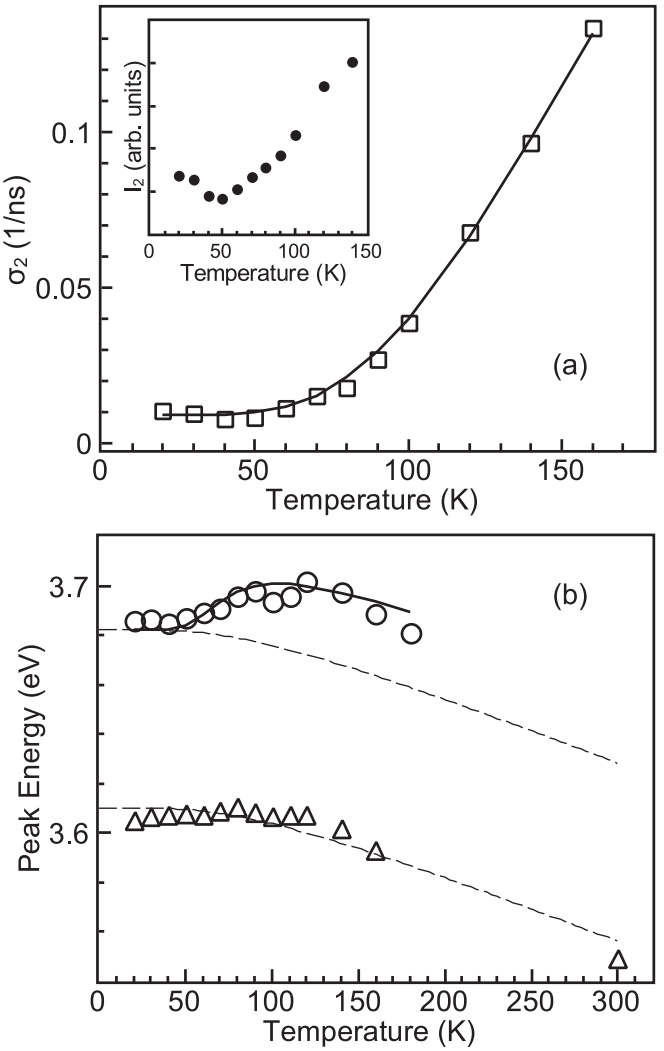

FIG. 7. (a) Temperature dependence of the decay rate of the high-energy component obtained in the analysis of the time profile. The inset shows the temperature dependence of the amplitude of the component. (b) Temperature dependence of the peak energies of low- and high-energy components. The dashed lines show the temperature dependence of the band-gap of the bulk ZnO, shifted in energy for the coincidence at low temperatures. The deviation of the high-energy component from the bulk band gap is accounted for by the thermal equilibrium model of dark and bright states.

from these states, and $\beta = (k_B T)^{-1}$. The factor γ is the ratio of the state densities and $\gamma = 1/3$ is adopted for the case of spin singlet and triplet, where the triplet state is the ground state. The solid line in the figure is the result of the numerical optimization for $\gamma = 1/3$. The optimized parameters are $\sigma_d = 0.0091\ \mathrm{ns}^{-1}$, $\sigma_b = 3.93\ \mathrm{ns}^{-1}$, and $\Delta E = 32$ meV. The line successfully reproduces the experimental result and justifies the applicability of the thermal equilibrium model of dark and bright states. The same parameters also explain the thermal variation of the peak energy of the high-energy component, as shown in Fig. 7(b). In the figure, the dashed lines show the temperature dependence of the band-gap of the bulk ZnO, shifted in energy for the coincidence at low temperatures.[24] The peak energy of the high-energy component deviates from the band-gap variation reflecting the increase of the bright

state luminescence at higher temperature, while the low-energy component follows the bulk band gap. It is well known that the electronic structures of the NCs are greatly affected by their shapes, and the assumption of $\gamma = 1/3$ used here may need to be modified. However, we find that the fitting is not sensitive to the value of γ, and a trial with $\gamma = 1$ gives about the same quality of fitting with slightly different parameters.

From the result in Fig. 7(b), it becomes clear that the bright exciton state lies about 100 meV higher than the low-energy component at T > 100 K. In addition, while not shown here, the high-energy component is observed to show a stronger thermal quenching than the low-energy component above 150 K, and the room-temperature PL spectrum becomes dominated by the low-energy component. These results indicate that the Stokes shift for the bright state should be 100 meV smaller than the value estimated in Fig. 2. Moreover, the full width of the PL spectrum is 180 meV at room temperature and is about 60 meV broader than the width at 20 K. This thermal broadening should be attributed to the phonon coupling and is partially responsible for the Stokes shift. The Stokes shift expected from the linewidth of 60 meV is 25 meV under the strong coupling approximation.[25] Therefore, the room-temperature Stokes shift of 135 meV, estimated from Fig. 2, is mostly explained by the trapping energy and the phonon-coupling energy, and hence the Stokes shift for the bright state is expected to be very small. The reasoning employed here may be too crude to conclude that the bright state is truly intrinsic, but it is at least probable that the trapping potential is very small compared to the confinement energy in the NCs that emit the high-energy component, and therefore the nature of the electronic states responsible for the luminescence should strongly reflect the intrinsic electronic structure of the ZnO NC.

The energy separation $\Delta E \sim 32$ meV for bright and dark states seems a bit large considering that only values around 10 meV are calculated for CdSe NCs,[6,7] and even smaller values are suggested.[9] Recently, the electronic states in spherical ZnO NCs were calculated under a pseudopotential framework.[11] The calculated result indicates that the exchange energy for a ZnO NC is around 5 meV for a spherical NC with 3 nm diameter. However, Efros *et al.* have shown in their calculation that the exchange splitting largely depends on the particle shape,[7] and it is known that many NCs of wurtzite semiconductors crystallize into ellipsoidal shape with its long axis parallel to the hexagonal c axis.[6,18,26,27] Therefore we think that the large energy splitting comes from the exchange energy of the excitonic state that is enhanced by the modified NC shape, although it cannot be justified in Fig. 1 because of the comparably poor resolution.

IV. CONCLUSIONS

We prepare high-quality ZnO nanocrystals by an alternative method including fast cooling and succeeding surface passivation by adding Mg salts. The TEM measurement shows that the crystal shape is almost spherical with an average diameter of about 3 nm, which is consistent with the calculated value from the absorption-edge energy. Time-resolved luminescence measurements performed at low temperature show a very slow luminescence component near the band edge with its lifetime around 0.1 μs. The temperature dependence of the luminescence peak energy and the lifetime are interpreted using the thermal equilibrium model of excitonic dark and bright states.

ACKNOWLEDGMENTS

The authors are deeply grateful to Dr. A. Ishizumi and the Kyoto-Advanced Nanotechnology Network for performing TEM measurements.

[1] K. Keis, E. Magnusson, H. Lindström, S. E. Lindquist, and A. Hagfeldt, Sol. Energy Mater. Sol. Cells **73**, 51 (2002).
[2] M. Boucharef, C. D. Bin, M. S. Boumaza, M. Colas, H. J. Snaith, B. Ratier, and J. Bouclé, Nanotechnology **21**, 205203 (2010).
[3] R. Könenkamp, R. C. Word, and M. Godinez, Nano Lett. **5**, 2005 (2005).
[4] T. Toyama, H. Takeuchi, D. Yamaguchi, H. Kawasaki, K. Itatani, and H. Okamoto, J. Appl. Phys. **108**, 84302 (2010).
[5] Y. Jin, J. Wang, B. Sun, J. C. Blakesley, and N. C. Greenham, Nano Lett. **8**, 1649 (2008).
[6] M. Nirmal, D. J. Norris, M. Kuno, M. G. Bawendi, Al. L. Efros, and M. Rosen, Phys. Rev. Lett. **75**, 3728 (1995).
[7] Al. L. Efros, M. Rosen, M. Kuno, M. Nirmal, D. J. Norris, and M. Bawendi, Phys. Rev. B **54**, 4843 (1996).
[8] S. A. Crooker, T. Barrick, and J. A. Hollingsworth, Appl. Phys. Lett. **82**, 2793 (2003).
[9] C. de Mello Donegá, M. Bode, and A. Meijerink, Phys. Rev. B **74**, 085320 (2006).
[10] B. Yang, J. E. Schneeloch, Z. Pan, M. Furis, and M. Achermann, Phys. Rev. B **81**, 073401 (2010).
[11] S. Baskoutas and G. Bester, J. Phys. Chem. C **114**, 9301 (2010).
[12] A. van Dijken, E. A. Meulenkamp, D. Vanmaekelbergh, and A. Meijerink, J. Lumin. **90**, 123 (2000).
[13] E. A. Meulenkamp, J. Phys. Chem. B **102**, 5566 (1998).
[14] H. Zhou, H. Alves, and D. M. Hofmann, Appl. Phys. Lett. **80**, 825 (2002).
[15] P. Y. Wu, J. Pike, F. Zhang, and S. W. Chan, Int. J. Appl. Ceram. Technol. **3**, 272 (2006).
[16] A. L. Patterson, Phys. Rev. **56**, 978 (1939).
[17] S. Yamamoto and T. Mishina, J. Lumin. **131**, 620 (2011).
[18] A. Wood, M. Giersig, M. Hilgendorff, A. Vilas-Campos, L. M. Liz-Marzán, and P. Mulvaney, Aust. J. Chem. **56**, 1051 (2003).
[19] A. van Dijken, A. H. Janssen, M. H. Smitsmans, D. Vanmaekelbergh, and A. Meijerink, Chem. Mater. **10**, 3513 (1998).
[20] J. F. Muth, R. M. Kolbas, A. K. Sharma, S. Oktyabrsky, and J. Narayan, J. Appl. Phys. **85**, 7884 (1999).
[21] S. Yamamoto, H. Yano, T. Mishina, and J. Nakahara, J. Lumin. **126**, 257 (2007).

[22] A. van Dijken, E. A. Meulenkamp, D. Vanmaekelbergh, and A. Meijerink, J. Phys. Chem. B **104**, 1715 (2000).
[23] D. C. Reynolds, D. C. Look, B. Jogai, and J. E. Hoelscher, J. Appl. Phys. **88**, 2152 (2000).
[24] H. D. Sun, T. Makino, N. T. Tuan, and Y. Segawa, Appl. Phys. Lett. **78**, 2464 (2001).
[25] K. W. Böer, *Survey of Semiconductor Physics* (Van Nostrand Reinhold, New York, 1990), p. 517.
[26] L. Guo, S. Yang, C. Yang, P. Yu, J. Wang, W. Ge, and G. K. L. Wong, Appl. Phys. Lett. **76**, 2901 (2000).
[27] V. A. Fonoberov and A. A. Balandin, Phys. Rev. B **70**, 195410 (2004).